


Modification of the Bose-Hubbard model parameters in an optical lattice by two-particle Wannier functions

Shou-Long Chen ^{*}

MOE Key Laboratory of Fundamental Physical Quantities Measurement, Hubei Key Laboratory of Gravitation and Quantum Physics, PGMF and School of Physics, *Huazhong University of Science and Technology*, Wuhan 430074, People's Republic of China



(Received 22 April 2024; accepted 28 August 2024; published 10 September 2024)

In systems with periodic potential fields, building relatively local Wannier functions can significantly simplify the Hamiltonian and enhance our understanding of the system's ground state and dynamic properties. In this work, we improve the current method of building the Wannier functions of ultracold atomic systems, including the case in the presence or absence of interactions. In noninteracting systems, we propose a method to directly obtain the real-valued maximally localized Wannier functions (MLWFs) by using real-valued eigenstates, and verify the effectiveness of this method in a two-dimensional (2D) degenerate system. In interacting systems, we obtain the effect of high-energy bands on the lowest-energy band by using the accurate calculation results of the two-particle system. In the two-particle system, we consider the effect of the entanglement between the particles and obtain the optimal two-particle Wannier functions. These Wannier functions are then further utilized to obtain the parameters of the extended Bose-Hubbard model. The effectiveness of the method is verified by taking a one-dimensional (1D) system with contact interaction as an example. In the three-particle and four-particle systems, compared calculation results with the original system and the unmodified two-band Bose-Hubbard model, we find that the effective Hamiltonian is more accurate than the unmodified two-band model. This verifies the effectiveness of our method, and the parameters obtained can reflect the original system well, which provides an effective method for accurate modeling of interacting systems.

DOI: [10.1103/PhysRevA.110.033312](https://doi.org/10.1103/PhysRevA.110.033312)

I. INTRODUCTION

With the development of laser technology and atom cooling technology, ultracold atoms can be loaded into various types of optical lattices, such as double-well lattice [1], honeycomb lattice [2], triangular lattice [3,4], Kagome lattice [5–7], artificial graphene [8,9], and more. The interaction between atoms can be adjusted by Feshbach resonance [10,11]. These ultracold atomic optical lattice systems are widely used in quantum simulations [12–14], quantum phase transitions [15–17], many-body interactions, quantum information processing [18,19], and quantum computation [20,21].

Theoretically, cold atoms in optical lattices are generally described by the Bose-Hubbard model [17,22,23]. The key parameters are the nearest-neighbor hopping and on-site interaction between particles, and these parameters are determined by the single-particle Wannier functions. Therefore, the first step to accurately model these systems is building appropriate local Wannier functions. Due to the $U(1)$ symmetry of Bloch functions, the Wannier functions are not unique. A well-known criterion is the maximum localization criterion introduced by Marzari and Vanderbilt [24] in solid-state physics, requiring that the built Wannier function has a minimum spatial extension. This method has been widely used in ultracold atomic systems [25–29]. Brouder *et al.* [30] proved

that MLWFs should be real if the system is topologically trivial, but the above methods rely on Bloch functions, so the variational space is complex and may fall into the local minimum of the complex number. Paul *et al.* [31] proposed to obtain the real-valued eigenstates by using discrete variable representation (DVR) and then obtain the real-valued Wannier functions by using the method proposed by Kivelson *et al.* [32]. Since the maximum localization criterion is not adopted, the resulting Wannier function has room for optimization.

Due to the interaction, Bloch functions are not the eigenstates of the system, so a set of Wannier functions is no longer an invariant subspace of the Hamiltonian. When the interaction is weak, the standard Bose-Hubbard model can accurately describe the properties of the system. When the interaction increases or long-range interactions (such as dipole interactions) are considered, this model will inevitably fail [33–38]. To describe the system accurately, it is necessary to modify the Bose-Hubbard model reasonably. Therefore, more Hamiltonian terms are introduced, such as next-nearest-neighbor hopping [39], density-induced tunneling [40,41], and pair tunneling [42–44], and the effects of higher-energy bands are considered, such as modifications of on-site interactions [45], multiband model [46,47], and three-body interaction [48–50]. Considering the effects of high-energy bands is a relatively complex process, and it is difficult to get accurate results. Many efforts have been made in this respect, such as modifying the Wannier functions [51,52], parameter comparison [53], and second-order perturbation theory [54]. Currently,

^{*}Contact author: 1554290407@qq.com

the methods of modifying the Wannier functions reflect the contribution of high orbits, but do not fully reflect the effect of multi-particle entanglement in interacting system.

In this article, we primarily focus on the above two points and propose potential methods for improvement. When interaction is not considered, we still use DVR to obtain real-valued eigenstates instead of Bloch functions, and then we adopt the maximum localization criterion to obtain the MLWFs. When interaction is considered, we use the idea of modifying the single-particle Wannier functions from the two-particle system in Ref. [52], and fully consider the effects of the entanglement of two-particle to obtain the two-particle Wannier functions, and then obtain the corresponding parameters for the extended Bose-Hubbard model.

Our article is organized as follows. In Sec. II, we first introduce some consensus on the Wannier functions in the non-interacting case. Then we introduce how to get the MLWFs in real space, including selecting the initial Wannier functions and optimizing the Wannier functions. Finally, the validity of this method is verified in a two-dimensional (2D) degenerate system. In Sec. III, we first introduce how to find the optimal two-particle Wannier functions in the interacting two-particle system, including the initialization and optimization of the two-particle Wannier functions, and how to use the two-particle Wannier functions to obtain the parameters of the extended Bose-Hubbard model. Then the above method is applied to one-dimensional (1D) system with contact interaction, and obtain the corresponding parameters of the extended Bose-Hubbard model. The calculations of energy spectrum and dynamics are carried out in three-particle and four-particle systems, and the results are compared with the original system and the unmodified two-band Bose-Hubbard model to verify the accuracy of the obtained parameters. Finally, we provide a summary and outlook in Sec. IV.

II. PERIODIC SYSTEMS WITHOUT INTERACTIONS

A. Wannier functions

For simplicity, we consider 1D periodic systems, the Hamiltonian can be written as $H = \frac{p_x^2}{2m} + V(x)$, where $V(x)$ is a potential field with period a . According to Bloch's theorem, the eigenstates are Bloch functions $|\varphi_{n,k}\rangle$, where n is the indication of the energy band and k is the quasimomentum

$$\varphi_{n,k}(x) = e^{-ikx} u_{n,k}(x), u_{n,k}(x) = u_{n,k}(x+a). \quad (1)$$

Assuming that the first l bands overlap, the relatively local generalized Wannier functions $|w_{n,R}\rangle$ can be obtained by Fourier transforming the Bloch functions of these bands

$$|w_{n,R}\rangle = \frac{1}{\sqrt{N}} \sum_{k,n'} e^{-ikR} U_{n',n}^{(k)} |\varphi_{n',k}\rangle, \quad (2)$$

where R represents the different unit cell, $U^{(k)}$ is a unitary matrix associated with the quasimomentum k , N is the total unit cell, and $1 \leq n, n' \leq l$. Because of the arbitrariness of $U_{n',n}^{(k)}$, the Wannier functions are not unique. From the above equation, we can also deduce that $|w_{n,R+1}\rangle = \hat{T}_a |w_{n,R}\rangle$, in which the operator \hat{T}_a represents the translation distance a along the x direction. if we make a unitary transformation of

the Wannier function

$$|w'_{n,R}\rangle = \sum_{i=1, j=1, m=1}^{i=l, j=l, m=N} \alpha_{i,j,m} \hat{A}_{i,j} \otimes \hat{T}_a^m |w_{n,R}\rangle, \quad (3)$$

and $\hat{A}_{i,j} |w_{n,R}\rangle = \delta_{j,n} |w_{i,R}\rangle$, where δ is the Dirichlet function. It can be verified that $|w'_{n,R}\rangle$ is still the Wannier function of these bands. Therefore, we can attribute the arbitrariness of the Wannier functions to the arbitrariness of $\{\alpha_{i,j,m}\}$. In other words, we need to find the most suitable $\{\alpha_{i,j,m}\}$ to get the MLWFs.

B. Maximally localized Wannier functions

To obtain the most appropriate $\{\alpha_{i,n,m}\}$, we adopt the method in Ref. [24], which is to minimize the spread of the Wannier functions, and the corresponding local functional is defined as

$$\Omega = \sum_n \langle w_{n,0} | \hat{x}^2 | w_{n,0} \rangle - \langle w_{n,0} | \hat{x} | w_{n,0} \rangle^2. \quad (4)$$

In prior work, they rewrote the above functional in k space and searched for the minimum by changing $U_{n',n}^{(k)}$ of Eq. (2). We know that MLWFs are real-valued when the system is topologically trivial. However, the prior methods rely on the Bloch functions, so the variational space will be complex and may fall into the local minimum of the complex number. In addition, in the optical lattice systems, we often obtain eigenstates by the DVR method, so they are always real-valued rather than Bloch functions. If we take these real-valued eigenstates as our starting point and restrict the variational space, that is, $\{\alpha_{i,j,m}\}$, to be real, then we not only reduce the variational space but also guarantee that the resulting Wannier functions are real. We can achieve this in the following two steps.

1. Step 1: Find an arbitrary set of real Wannier functions

We assume that there are l Bloch band energy spectrum overlapping together, and label these eigenstates of position representation as $\vec{\varphi}$. Our goal is to find a set of real Wannier functions \vec{w}_{tar} such that they represent the same Hilbert space as $\vec{\varphi}$. We can start from an initial set of Wannier functions \vec{w}_{ini} and gradually iterate to approximate the target Wannier functions \vec{w}_{tar} . In the $\vec{\varphi}$, the eigenstates with $k=0$ are the easiest to identify, they are real and the distribution of wave function in each unit cell is the same. Therefore, we can intercept the wave function of the eigenstate with $k=0$ in each unit cell. After normalization, each wave function that is intercepted is an element of the initial Wannier functions \vec{w}_{ini} .

Next, we use $\vec{\varphi}$ to modify \vec{w}_{ini} . We first calculate the degree of coincidence of the Hilbert space of $\vec{\varphi}$ and \vec{w}_{ini} ,

$$M_{i,j} = \langle \varphi_i | w_j \rangle, \quad (5)$$

where $|\varphi_i\rangle$ represents the i th element in $\vec{\varphi}$, and $|w_j\rangle$ represent the j th element in \vec{w}_{ini} . If the matrix M is not unitary, it indicates that the Hilbert spaces represented by $\vec{\varphi}$ and \vec{w}_{ini} are inconsistent, then, we should adjust $\vec{\varphi}$ and \vec{w}_{ini} according to matrix M . To keep the Hilbert space described by the modified $\vec{\varphi}$ unchanged, the matrix M must be modified to be unitary. Commonly used methods include the Löwdin orthogonalization [55] and the Schmidt orthogonalization [56]. The

calculation efficiency of Löwdin orthogonalization is high, but the error of numerical calculation will increase rapidly when the eigenvalue of the matrix approaches zero. For the stability of the calculation, we adopt the Schmidt orthogonalization.

When the matrix M is unitary, we update $\bar{\varphi}$ and \bar{w}_{ini} ,

$$\bar{\varphi}_{\text{new}} = M\bar{\varphi}_{\text{old}}, \quad (6)$$

$$\bar{w}_{\text{ini}} = \bar{\varphi}_{\text{new}}. \quad (7)$$

\bar{w}_{ini} obtained from Eq. (7) generally does not satisfy translational symmetry and needs to be modified appropriately. An efficient method is to translate all Wannier functions in \bar{w}_{ini} to the first unit cell and add these states to obtain new Wannier functions $|w_{n,\text{new}}\rangle$, and then translate these new Wannier functions $|w_{n,\text{new}}\rangle$ to each unit cell to obtain \bar{w}_{ini} satisfying translation symmetry. The specific operation is as follows:

$$|w_{n,\text{new}}\rangle = \sum_{R=1}^{R=N} \hat{T}_a^{1-R} |w_{n,R}\rangle, \quad |w_{n,R}\rangle = \frac{\hat{T}_a^{R-1} |w_{n,\text{new}}\rangle}{\sqrt{\langle w_{n,\text{new}} | w_{n,\text{new}} \rangle}}. \quad (8)$$

This also applies to two-dimensional and higher-dimensional systems, because translation operators in different directions are commutative. We can perform the similar operation as Eq. (8) in each direction to make each Wannier function to the first unit cell and get $|w_{n,\text{new}}\rangle$, and finally perform the inverse procedure to obtain \bar{w}_{ini} with translation symmetry. Next, we use the \bar{w}_{ini} obtained from the above equation as a new starting point and repeat the above process from Eq. (5) until the matrix M obtained from Eq. (5) becomes the identity matrix. The resulting \bar{w}_{ini} is our target Wannier functions \bar{w}_{tar} .

The specific process of the above method can be simply summarized as follows: In the first step, we use the numerical calculation to obtain the eigenstates $\bar{\varphi}$ and give the initial Wannier functions \bar{w}_{ini} . In the second step, Eq. (5) is used to calculate the degree of coincidence of the Hilbert space represented by $\bar{\varphi}$ and \bar{w}_{ini} . When they do not coincide exactly, $\bar{\varphi}$ and \bar{w}_{ini} are modified using Eqs. (6), (7), and (8). In the third step, the above two steps are repeated until the Hilbert space represented by $\bar{\varphi}$ and \bar{w}_{ini} coincide. It should be noted that in the first few iterations, we do not need to update \bar{w}_{ini} with Eqs. (7) and (8), which can ensure that the Wannier functions \bar{w}_{tar} are relatively local at the end.

2. Step 2: Obtain the MLWFs

Now, we combine Eqs. (3) and (4) to update the Wannier functions \bar{w}_{tar} . Because we require the transformation matrix to be unitary, the $\alpha_{i,j,m}$ in Eq. (3) needs to satisfy additional restrictions. To avoid additional constraint equations, we adopt the equivalent exponential form

$$\begin{aligned} |w'_{n,R}\rangle &= e^{\sum_{i=1,j=1,m=1}^{i=l,j=l,m=N} \alpha_{i,j,m} (\hat{A}_{j,i} \otimes \hat{T}_a^m - \hat{A}_{i,j} \otimes \hat{T}_a^{-m})} |w_{n,R}\rangle \\ &= \hat{T}_g |w_{n,R}\rangle. \end{aligned} \quad (9)$$

The operator $\hat{A}_{i,j}$, written in matrix form, is a $l \times l$ zero matrix with value of 1 only in the (i, j) th element. It is not difficult to find that the operators \hat{T}_g are unitary operators. Because it is calculated in position space, to avoid boundary effects, we choose the Wannier function located in the middle unit cell R

as the starting point. Substituting Eq. (9) into Eq. (4), we have

$$\Omega = \sum_{n=1}^{n=l} \langle w_{n,R} | \hat{T}_g^\dagger \hat{x}^2 \hat{T}_g | w_{n,R} \rangle - \langle w_{n,R} | \hat{T}_g^\dagger \hat{x} \hat{T}_g | w_{n,R} \rangle^2. \quad (10)$$

Since $\hat{A}_{j,i} \otimes \hat{T}_a^m$ and \hat{T}_g are not commutative, we cannot obtain the derivative of Ω concerning $\alpha_{i,j,m}$ for any $\{\alpha_{i,j,m}\}$. However, obviously, it's easy to get the derivative for $\{\alpha_{i,j,m}\} = 0$. Let

$$\overline{XX}_{i,j} = w^\dagger(i) \hat{x}^2 \bar{w}(j), \quad X_{i,j} = \bar{w}^\dagger(i) \hat{x} \bar{w}(j), \quad (11)$$

where $\bar{w}(i) = |w_{\text{int}[1+(i-1)/N], i-N \times \text{int}[(i-1)/N]}\rangle$ and the function $\text{int}()$ represents to get the integer part of a real number. Then, we have

$$\begin{aligned} \left. \frac{\partial \Omega}{\partial \alpha_{i,j,m}} \right|_{\alpha=0} &= \sum_{n=1}^{n=l} \langle n, R | [A_{i,j} \otimes T_a^{-m} - A_{j,i} \otimes T_a^m, \overline{XX}] | n, R \rangle \\ &\quad - 2 \langle n, R | X | n, R \rangle \langle n, R | [A_{i,j} \otimes T_a^{-m} - A_{j,i} \otimes T_a^m, X] \\ &\quad \times | n, R \rangle. \end{aligned} \quad (12)$$

$|n, R\rangle$ represents the R th basis vector in the n th band and it is a Nl zero vector with value of 1 only in the $[N(n-1) + R]$ th element. To obtain the MLWFs, we must ensure that the above equation is equal to 0 for all $\alpha_{i,j,m}$. When the above equation is not equal to 0, we need to use the gradient descent method to gradually decrease Ω . For the p th iteration, we set

$$\alpha_{i,j,m}^p = -\lambda \left. \frac{\partial \Omega}{\partial \alpha_{i,j,m}} \right|_{\alpha=0}, \quad (13)$$

$$T_p = e^{\sum_{i=1,j=1,m=1}^{i=l,j=l,m=N} \alpha_{i,j,m}^p (A_{j,i} \otimes T_a^m - A_{i,j} \otimes T_a^{-m})}, \quad (14)$$

where λ is a real number from 0 to 1. After each iteration, we update \overline{XX} and X ,

$$\overline{XX}_{\text{new}} = T_p^\dagger \overline{XX}_{\text{old}} T_p, \quad X_{\text{new}} = T_p^\dagger X_{\text{old}} T_p. \quad (15)$$

Assume that the derivative of Ω is 0 after P iterations, we have

$$\bar{w}_{\text{final}} = \prod_{p=1}^{p=P} T_p \bar{w}_{\text{tar}}, \quad (16)$$

the corresponding effective Hamiltonian H_{eff} can be written as

$$H_{\text{eff},i,j} = \bar{w}_{\text{final}}^\dagger(i) \hat{H} \bar{w}_{\text{final}}(j). \quad (17)$$

Inevitably, if the target Wannier functions \bar{w}_{tar} are not selected properly, the convergent Ω may not be the global minimum. We need to repeat the above steps starting with *step 1*. The initial Wannier functions \bar{w}_{ini} in *step 1* is set to the \bar{w}_{final} obtained from Eq. (16), but only the wave function of the unit cell with the highest probability is retained, and the wave function of other unit cells is set to 0. If the two optimization results are equal, then this is the optimal basis vector that can be obtained by this method.

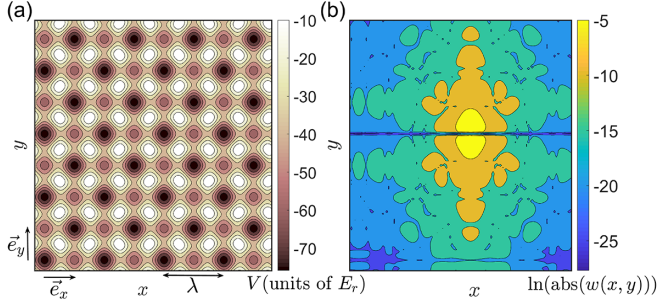


FIG. 1. (a) The checkerboard potential field when $V_1 = 32.8E_r$. Each unit cell consists of a deep and a shallow well. The color indicates strength, and the unit is the recoil kinetic energy E_r . (b) Contour plot for one of the MLWFs of p_y orbital. The color in the figure stands for the logarithm of the absolute value of this Wannier function, with the corresponding parameter values $V_1 = 32.8E_r$ and $\beta = 0.4375\pi$.

C. Example

Here, we use a 2D optical lattice system to illustrate the validity of our method, and the Hamiltonian is

$$H_0 = -\frac{\hbar^2}{2m}(\partial_x^2 + \partial_y^2) + V(x, y), \quad (18)$$

$$V(x, y) = -|V_1| \cos(kx) + e^{i\beta} \cos(ky)|^2. \quad (19)$$

This kind of potential field has been studied experimentally and theoretically [57,58]. V_1 and β are adjustable parameters. When $\beta = \frac{\pi}{2}$, the system can be decomposed into two independent 1D systems. To couple the potential fields in x and y directions, we set the parameter β to deviate from $\frac{\pi}{2}$. Due to the limitation of computing resources, we consider four periods in the x and y directions, respectively.

Figure 1(a) shows the potential field of the calculated system, which contains 32 unit cells. Under appropriate parameters, the first energy band consists of the s orbital of the deep well, and the second energy band consists of three Bloch bands corresponding to the s orbital of the shallow well and the p_x and p_y orbitals of the deep well. Our goal is to get the MLWFs for the second energy band and write the effective Hamiltonian of this energy band under these localized basis vectors. In Fig. 1(b), we show one of the MLWFs of p_y orbital obtained by the above method. The color represents the logarithm of the absolute value of the wave function, and it can be seen that it decays exponentially with distance. Using the obtained MLWFs, we get the corresponding effective Hamiltonian by numerical calculation. As the distance between the two unit cells increases, the hopping decays exponentially, so we only keep partly significant values. We label three different MLWFs by $\{s, x, y\}$, and this energy band can be accurately described by the following Hamiltonian:

$$\begin{aligned} H_{\text{eff}} = & J_{\text{sp}} \sum_{\mu, \vec{r}} [\hat{a}_{\mu, \vec{r}}^\dagger \hat{a}_{s, \vec{r} + \vec{e}_\mu} + \text{H.c.}] \\ & + J_{\parallel} \sum_{\mu, \vec{r}} [\hat{a}_{\mu, \vec{r}}^\dagger \hat{a}_{\mu, \vec{r} + \vec{e}_x + \vec{e}_y} + \hat{a}_{\mu, \vec{r}}^\dagger \hat{a}_{\mu, \vec{r} + \vec{e}_x - \vec{e}_y} + \text{H.c.}] \\ & + J_{\perp} \sum_{\mu, \vec{r}} [\hat{a}_{\mu, \vec{r}}^\dagger \hat{a}_{\mu', \vec{r} + \vec{e}_x + \vec{e}_y} + \hat{a}_{\mu, \vec{r}}^\dagger \hat{a}_{\mu', \vec{r} + \vec{e}_x - \vec{e}_y} + \text{H.c.}] \end{aligned}$$

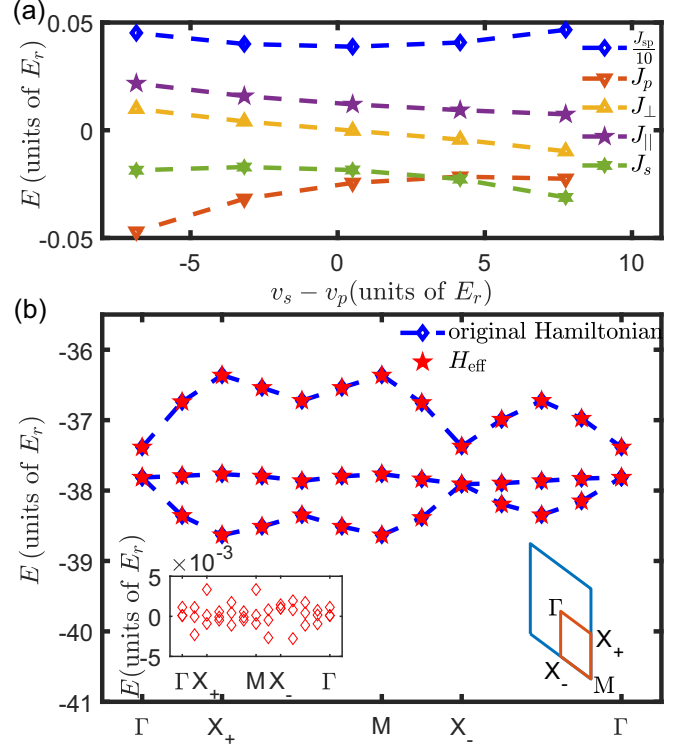


FIG. 2. (a) Plot of the tunneling coefficients in Eq. (20) as a function of $v_s - v_p$ for $V_1 = 34.6E_r$, the corresponding β is $(0.4625, 0.4500, 0.4375, 0.4250, 0.4125)\pi$. (b) The energy spectrum of the effective Hamiltonian H_{eff} and the original Hamiltonian, where $V_1 = 34.6E_r$ and $\beta = 0.4375\pi$. The inset on the right shows the Brillouin zone of the system and the points shown in (b) fall on the red line. The inset on the left shows the difference between the eigenvalues of H_{eff} and the original Hamiltonian in (b).

$$\begin{aligned} & + J_p \sum_{\mu, \vec{r}} [\hat{a}_{\mu, \vec{r}}^\dagger \hat{a}_{\mu, \vec{r} + 2\vec{e}_\mu} + \text{H.c.}] \\ & + J_s \sum_{\mu, \vec{r}} [\hat{a}_{s, \vec{r}}^\dagger \hat{a}_{s, \vec{r} + 2\vec{e}_\mu} + \text{H.c.}] \\ & + (v_s - v_p) \sum_{\vec{r}} \hat{a}_{s, \vec{r}}^\dagger \hat{a}_{s, \vec{r}}, \quad (20) \end{aligned}$$

where $\hat{a}_{\mu, \vec{r}}^{(\dagger)}$ and $\hat{a}_{s, \vec{r}}^{(\dagger)}$ are bosonic annihilation (creation) operators for p_μ ($\mu = \{x, y\}$, $\mu' = \{y, x\}$) and s orbitals at unit cell position \vec{r} . \vec{e}_x and \vec{e}_y are unit vectors, shown in Fig. 1(a). Because $v_s - v_p$ changes too fast with β , Fig. 2(a) illustrates the variation of the other parameters with $v_s - v_p$. The energy unit is the recoil energy $E_r = \frac{\hbar^2 k^2}{2m}$. Figure 2(b) shows the energy spectrum of the effective Hamiltonian H_{eff} and the original Hamiltonian. The inset on the right shows the difference between the eigenvalues of these two Hamiltonian calculations, which is very small, indicating that the effective Hamiltonian describes the original Hamiltonian well.

III. PERIODIC SYSTEMS WITH INTERACTIONS

A. Two-particle Wannier functions

When the system has interaction, the system is usually written as a Bose-Hubbard model by using the Wannier

functions of the lowest-energy band. This method ignores the coupling of the lowest-energy band and higher-energy bands, and with the increase of the interaction, it will introduce a larger error. To solve this problem, based on Ref. [52] and fully considering the effect of two-particle entanglement, we propose a method to modify the parameters of the Bose-Hubbard model by using the calculation results of the two-particle system.

For simplicity, we study 1D boson systems with interactions, and potential field $V(x)$ satisfies $V(x) = V(x+a)$. The Hamiltonian of the two-particle system is

$$H = -\frac{\hbar^2}{2m}(\partial_{x_1}^2 + \partial_{x_2}^2) + V(x_1) + V(x_2) + I(|x_1 - x_2|). \quad (21)$$

First, we need to get the eigenstates of the lowest-energy band. We use the MLWFs of the system at zero interactions, which are assumed to be known, as the basis vectors for the Hamiltonian, which needs to be written in a quadratic quantized form due to the boson system. We only care about getting the information of the lowest-energy band accurately, so we do not need to use all Wannier functions to save computing resources.

Next, we describe the method of obtaining the effective parameters of the lowest-energy band in detail, and label the lowest-energy band as s . In this two-particle system, there is still the translational symmetry $\hat{T}_{2,a}$ [59], that is, when two particles are translated by a distance of a simultaneously, the Hamiltonian remains unchanged. This symmetry will play a key role in the subsequent search for the effective Hamiltonian.

Our goal is to obtain the optimal basis vector $|w_{i,j}\rangle$ (in the noninteracting limit, $|w_{i,j}\rangle \propto a_i^\dagger a_j^\dagger |0\rangle$, where a_i^\dagger is the creation operator for the i th MLWFs of the s band), and we have reason to believe that it should be dominated by the corresponding Fock state $a_i^\dagger a_j^\dagger |0\rangle$. We will take advantage of this by requiring $|w_{i,j}\rangle$ to have the maximum projection on the corresponding Fock state $a_i^\dagger a_j^\dagger |0\rangle$.

Our method consists of two steps. The first step is to find a set of the target two-particle Wannier functions \bar{w}_{tar} that satisfies the symmetry $\hat{T}_{2,a}$, and the method for this step is similar to the noninteracting method. First, we use exact diagonalization to obtain the eigenstates of the system, and select the eigenstates we need. In our case, we need to select the eigenstates $|\varphi\rangle$ with the probability of s orbital greater than 50%, that is, $\langle \varphi | \sum_i a_i^\dagger a_i | \varphi \rangle > 1$, and label these states as $\bar{\varphi}$. Next, we choose the initial two-particle Wannier functions \bar{w}_{ini} , which could be $|w_{i,j}\rangle \propto a_i^\dagger a_j^\dagger |0\rangle$. For the convenience of calculation, we need to rearrange the elements of vectors \bar{w}_{ini} according to the invariant subspace of operator $\hat{T}_{2,a}$,

$$\bar{w}_{\text{ini}} = \begin{pmatrix} \bar{w}_1 \\ \bar{w}_2 \\ \dots \\ \bar{w}_k \end{pmatrix}, \quad \hat{T}_{2,a}|w_{j,l}\rangle = |w_{j,l+1}\rangle, \quad (22)$$

where j and l denote the l th element in vector \bar{w}_j , and k is the number of invariant subspaces of operator $\hat{T}_{2,a}$ in the \bar{w}_{ini} . Then, calculate the coincidence degree of the Hilbert space represented by \bar{w}_{ini} and $\bar{\varphi}$,

$$M_{i,j} = \langle \varphi_i | w_j \rangle, \quad (23)$$

where $|\varphi_i\rangle$ represents the i th element in $\bar{\varphi}$, and $|w_j\rangle$ represent the j th element in \bar{w}_{ini} . If the matrix M is not unitary, we will use Schmidt orthogonalization to change it into a unitary matrix. Then, we update $\bar{\varphi}$ and \bar{w}_{ini} ,

$$\bar{\varphi}_{\text{new}} = M\bar{\varphi}_{\text{old}}, \quad (24)$$

$$\bar{w}_{\text{ini}} = \bar{\varphi}_{\text{new}}. \quad (25)$$

The \bar{w}_{ini} obtained from the above equation does not necessarily satisfy $\hat{T}_{2,a}$ symmetry. We can follow Eq. (8) and perform the following operation for each invariant subspace of $\hat{T}_{2,a}$ in \bar{w}_{ini} :

$$|w_{j,\text{new}}\rangle = \sum_l \hat{T}_{2,a}^{l-1} |w_{j,l}\rangle, \quad |w_{j,l}\rangle = \frac{\hat{T}_{2,a}^{l-1} |w_{j,\text{new}}\rangle}{\sqrt{\langle w_{j,\text{new}} | w_{j,\text{new}} \rangle}}, \quad (26)$$

and the definition of j and l refers to Eq. (22). We use the \bar{w}_{ini} obtained from the above equation as a new starting point and repeat the above process from Eq. (23) until the matrix M obtained from Eq. (23) becomes the identity matrix. The resulting \bar{w}_{ini} is our target Wannier functions \bar{w}_{tar} . It should be noted that we do not perform Eqs. (25) and (26) in the process of the first few iterations.

In the second step, we require that the two-particle Wannier function [52,59] in the \bar{w}_{tar} is as similar as possible to the corresponding Fock state $|w'_{i,j}\rangle \propto a_i^\dagger a_j^\dagger |0\rangle$. We label these Fock states as \bar{w}' , and refer to Eq. (22) to reorder the Fock states in \bar{w}' according to the invariant subspace of symmetry $\hat{T}_{2,a}$. According to the previous work [60], the corresponding variational function can be defined as

$$\Omega = \sum_{j=1}^k |\langle w_{j,1} | w'_{j,1} \rangle|^2, \quad (27)$$

where k is the number of invariant subspaces of operator $\hat{T}_{2,a}$ in the \bar{w}' . Then, we can define unitary operators

$$\hat{T} = e^{\sum_{i=1}^k \sum_{j=1}^k \sum_{m=1}^N \alpha_{i,j,m} (\hat{A}_{j,i} \otimes \hat{T}_{2,a}^m - \hat{A}_{i,j} \otimes \hat{T}_{2,a}^{-m})}, \quad (28)$$

where $\hat{A}_{j,i}$ represents the mapping from the i th invariant subspace to the j th invariant subspace, $\hat{A}_{j,i}|w_{n,l}\rangle = \delta_{i,n}|w_{j,l}\rangle$, and N is the total unit cells. Every subspace has N basis vectors, except when N is even, there is a subspace with $N/2$ basis vectors. Any two possible two-particle Wannier functions can be connected by the above unitary operator \hat{T} , so we can find the optimal $\alpha_{i,j,m}$ that maximizes the value of Ω by variation. We define the coupling matrix O ,

$$O_{i,j} = \langle w_i | w'_j \rangle, \quad (29)$$

where i represents the i th element in \bar{w}_{tar} and j represents the j th element in \bar{w}' . We describe the each element in \bar{w}_{tar} or \bar{w}' in two ways, for example, the $(N+1)$ th element $|w_{N+1}\rangle$ in \bar{w}_{tar} can also be written as $|w_{2,1}\rangle$ to represent the first element in \bar{w}_2 . Then, we have

$$\Omega = \sum_{n=1}^{n=k} |\langle n, 1 | T^\dagger O | n, 1 \rangle|^2, \quad (30)$$

where $|n, 1\rangle$ is a $N(N-1)/2$ zero vector with a value of 1 only in the $[N(n-1)+1]$ th element. Because the operators

$\hat{A}_{j,i} \otimes \hat{T}_{2,a}^m$ and \hat{T} are not commutative, we can only take the derivative at $\alpha = 0$,

$$\begin{aligned} \left. \frac{\partial \Omega}{\partial \alpha_{i,j,m}} \right|_{\alpha=0} &= \sum_{n=1}^k \langle n, 1 | O | n, 1 \rangle \\ &\times \langle n, 1 | (A_{i,j} \otimes T_{2,a}^{-m} - A_{j,i} \otimes T_{2,a}^m) O | n, 1 \rangle \\ &+ \text{H.c.} \end{aligned} \quad (31)$$

When the above equation is not equal to 0, we need to use the gradient ascent method to gradually increase Ω . For the p th iteration, we set

$$\begin{aligned} \alpha_{i,j,m}^p &= \lambda \left. \frac{\partial \Omega}{\partial \alpha_{i,j,m}} \right|_{\alpha=0}, \quad (32) \\ T_p &= e^{\sum_{i=1}^k \sum_{j=1}^k \sum_{m=1}^N \alpha_{i,j,m}^p (A_{j,i} \otimes T_{2,a}^m - A_{i,j} \otimes T_{2,a}^{-m})}, \quad (33) \end{aligned}$$

where λ is a real number from 0 to 1. After each iteration, we update O ,

$$O_{\text{new}} = T_p^\dagger O_{\text{old}}, \quad (34)$$

and assume that the derivative of Ω is 0 after P iterations, we have

$$\vec{w}_{\text{final}} = \prod_{p=1}^{p=P} T_p \vec{w}_{\text{tar}}. \quad (35)$$

The corresponding effective Hamiltonian H_s can be written as

$$H_{s,i,j} = \langle w_{\text{final},i} | \hat{H} | w_{\text{final},j} \rangle. \quad (36)$$

Finally, we use the obtained Hamiltonian H_s to get the parameters of the effective two-body Hamiltonian terms. We assume that the single-body Hamiltonian terms H_0 are invariant and known and calculate $H_{\text{remain}} = H_s - H_0$. The equivalent two-body interaction terms and corresponding parameters can be obtained by rewriting the matrix H_{remain} in the form of the quadratic quantization.

B. Example

We take the bosons with contact interaction in the 1D optical lattice as an example, and obtain the extended Bose-Hubbard model and the corresponding parameters by using the above method. We show the effectiveness of our method by comparing energy spectrum and dynamic evolution of the effective Hamiltonian and the original Hamiltonian. Compared with the calculation results of the two-band model without considering the parameter modification, it shows that the effective Hamiltonian is more accurate. In addition, the Hilbert space of the effective Hamiltonian is smaller, the computation will be more efficient.

Following the above method, we consider the system with two bosons, and the Hamiltonian of the system is

$$H = \sum_{x=x_1, x_2} \left[-\frac{\hbar^2}{2m} \partial_x^2 + V \cos^2(kx) \right] + g\delta(x_1 - x_2), \quad (37)$$

where V is the potential field strength and g is the contact interaction strength. Both of them are adjustable parameters, in units of recoil energy $E_R = \frac{\hbar^2 k^2}{2m}$. The number of periods

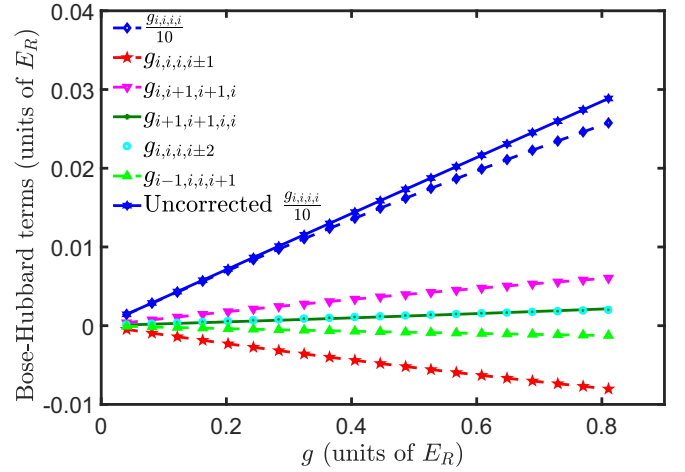


FIG. 3. The parameters in Eq. (38) vary with the interaction strength g . We add uncorrected on-site interactions as a contrast. The potential well depth of the optical lattice is $V = 5E_R$.

of the potential well is $N = 6$. Then we get the Wannier functions of the first few energy bands when $g = 0$. It is worth noting that the more you use the Wannier functions, the more accurate the calculated value will be. Because we need to verify it in the multiparticle system later, we choose to obtain the Wannier functions of only the first four energy bands. Next, the energy spectrum and eigenstates of the lowest-energy band are obtained by exactly diagonalizing the Hamiltonian under the Wannier functions. Finally, the optimal two-particle Wannier functions are found by using the above method. By using the Hamiltonian under these two-particle Wannier functions, the parameters of the two-body operator are obtained by comparing with the Hamiltonian when $g = 0$.

Keeping the relatively significant terms, the effective Hamiltonian of the first energy band of the system can be written as

$$\begin{aligned} H_s &= H_0 + \sum_i \left[\frac{g_{i,i,i,i}}{2} \hat{a}_i^\dagger \hat{a}_i^\dagger \hat{a}_i \hat{a}_i + \frac{g_{i,i+1,i+1,i}}{2} \hat{a}_i^\dagger \hat{a}_{i+1}^\dagger \hat{a}_{i+1} \hat{a}_i \right] \\ &+ \sum_i \left[\frac{g_{i,i,i,i±1}}{2} \hat{a}_i^\dagger \hat{a}_i^\dagger \hat{a}_i \hat{a}_{i±1} + \frac{g_{i-1,i,i,i+1}}{2} \hat{a}_{i-1}^\dagger \hat{a}_i^\dagger \hat{a}_i \hat{a}_{i+1} \right] \\ &+ \frac{g_{i,i,i,i±2}}{2} \hat{a}_i^\dagger \hat{a}_i^\dagger \hat{a}_i \hat{a}_{i±2} + \frac{g_{i+1,i+1,i,i}}{2} \hat{a}_{i+1}^\dagger \hat{a}_{i+1}^\dagger \hat{a}_{i+1} \hat{a}_i + \text{H.c.}, \end{aligned} \quad (38)$$

where H_0 is the known single-body Hamiltonian. The first two terms represent on-site and nearest-neighbor interactions and the last four terms represent tunneling due to density. If they are not corrected by higher-energy bands, their values can be directly obtained by calculating overlap integrals of the interaction term using the Wannier functions, they are proportional to the interaction strength. In Fig. 3, we show how the parameters in Eq. (38) change with the strength of the interaction when considering the effects of high-energy bands, specifically adding the on-site interaction without the modification as a comparison. We can see that under the effects of the high-energy bands, the greater the interaction

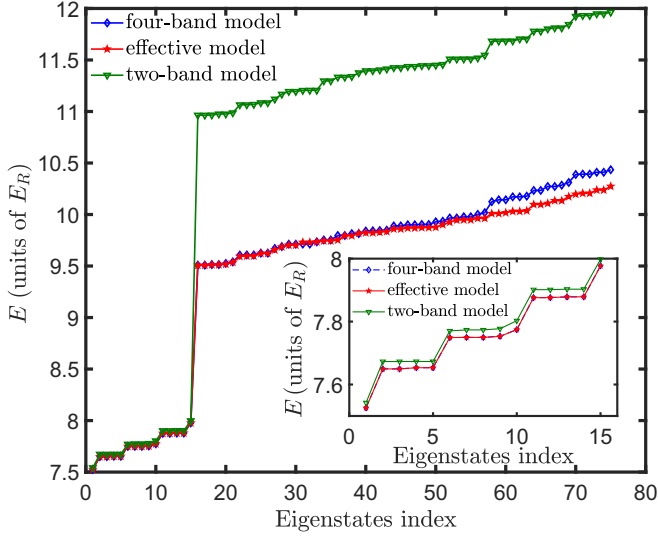


FIG. 4. Partial energy spectra of the four-band model, the effective model, and the two-band model in the four-particle system, where the interaction strength $g = 0.45E_R$ and the potential well depth $V = 5E_R$. The inset enlarges the energy spectrum of the first 15 eigenstates.

is, the greater the correction is needed, and the absolute value is smaller than that without the modification.

Next, we will verify the validity of the parameters in the three and four-particle systems by comparing energy spectrum and dynamics evolution with the original system and the two-band Bose-Hubbard model. In the original system, we consider six potential wells. In the process of computational dynamics, we use the four-band model as the approximate Hamiltonian, and mark the dynamic evolution of states in this Hamiltonian as $|\psi_4(t)\rangle$. The similar $|\psi_1(t)\rangle$ and $|\psi_2(t)\rangle$ are used to mark the dynamic evolution where only one band and two bands are considered. In addition, the dynamic evolution of the state computed by the effective Hamiltonian H_s is denoted $|\psi_s(t)\rangle$. Finally, we project all states into the Hilbert space of the lowest energy band, that is, $|\psi_4(t)\rangle \Rightarrow |\psi_4(t) \rightarrow 1\rangle$ and $|\psi_2(t)\rangle \Rightarrow |\psi_2(t) \rightarrow 1\rangle$. We calculated the occupancy probabilities of these states in the lowest band as $P_4(t) = \langle \psi_4(t) \rightarrow 1 | \psi_4(t) \rightarrow 1 \rangle$ and $P_2(t) = \langle \psi_2(t) \rightarrow 1 | \psi_2(t) \rightarrow 1 \rangle$, and the similarity between these states and $|\psi_4(t) \rightarrow 1\rangle$ is calculated as $f_s(t) = |\langle \psi_4(t) \rightarrow 1 | \psi_s(t) \rangle|^2 / P_4(t)$, $f_1(t) = |\langle \psi_4(t) \rightarrow 1 | \psi_1(t) \rangle|^2 / P_4(t)$ and $f_2(t) = |\langle \psi_4(t) \rightarrow 1 | \psi_2(t) \rangle|^2 / P_4(t) / P_2(t)$. This gives a quantitative way to compare the effectiveness of effective models.

In the three-particle system, we choose two initial states, the first is $|1, 0, 1, 0, 1, 0\rangle$ and the second is $|2, 1, 0, 0, 0, 0\rangle$. The influence of the interaction on these two initial states is increasing gradually. In the four-particle system, the initial states we choose are $|1, 1, 0, 1, 0, 1\rangle$ and $|2, 1, 1, 0, 0, 0\rangle$. In Fig. 4, we draw the energy spectrum of the first 75 eigenstates of the effective model, the two-band model and the four-band model in the four-particle system, where the first 15 eigenstates are mainly contributed by the single-occupied states and the last 60 states are contributed by the double-occupied states. The inset magnifies the energy spectrum comparison

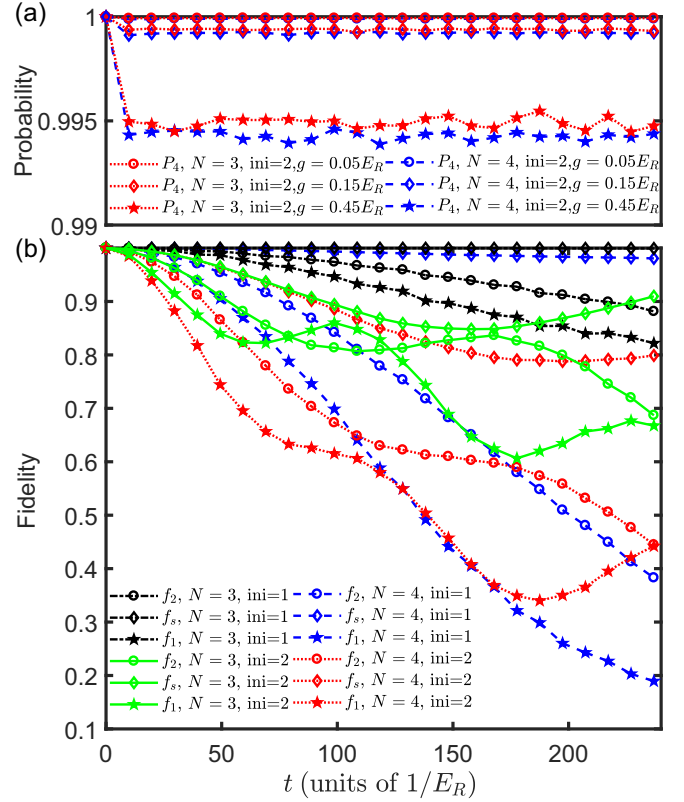


FIG. 5. (a) The projected probability of the dynamic calculation results in the lowest band for the four-band model. N is the particle number, $ini = 2$ indicates that the initial state is the second initial state, and g is the interaction strength. (b) Comparison of the dynamic calculation results of each model with the four-band model. f_s represents the effective model, f_2 represents the two-band model, and f_1 represents the single-band model. Strength of interaction g is $0.45E_R$.

results of the first 15 states. In the eigenstates contributed by the single-occupied states, the energy spectrums of the effective and four-band models are almost the same, while the energy spectrum of the two-band and four-band models are somewhat different. In the eigenstates contributed by the dual-occupied states, the energy spectrum of the two models is different from that of the four-band model, but the effective model is closer to the four-band model. Figure 5(a) shows the change of the occupancy probability of the four-band model in the first band with time under different interactions. We can see that as the increase of interaction, the probability of occupation of higher-energy bands also increases gradually. Figure 5(b) shows the similarity of the dynamics evolution of other models and the dynamics evolution of the four-band model under different initial states and interactions. We can see that the higher the number of particles, the lower the fidelity, but in all the test cases, the result of the effective Hamiltonian is closer to the four-band model than the two-band model. The results show that the parameters obtained by this method can effectively reflect the properties of the real system, and considering the modification of parameters cannot only improve the accuracy but also greatly reduce the calculation time compared with directly building the multi-band model.

IV. CONCLUSION AND OUTLOOK

In conclusion, we propose a more rigorous method for modeling boson optical lattice systems. This method involves two improvements. The first improvement is to adopt the maximum localization criterion to directly obtain the real-valued MLWFs based on the real-valued eigenstates obtained by using the DVR method in the case of no interaction. The second improvement is that in the presence of interactions, we additionally consider the effect of particle entanglement on the lowest-energy band on the basis of considering the effect of higher energy band on the Wannier functions of the lower-energy band. To achieve this goal, we extract the information of the lowest band and obtain the effective two-particle Wannier functions based on the local single-particle Wannier functions and the strict calculation results using the two-particle model. Finally, the values of the parameters in the effective Hamiltonian are calculated by using the two-particle Wannier functions. Compared with the dynamic calculation results of the original system and the two-band model, the effectiveness and relative accuracy of this method are verified, which provides an effective method for the accurate study of interacting systems.

As for the outlook, our current study primarily focuses on the modification of two-body interactions by particle

entanglement, and without accounting for the effective three-body interactions that should exist in the system, which has been proved by many works [48–50]. Therefore, the effect of particle entanglement on the three-body interactions can be considered next, and the effective three-particle Wannier functions need to be obtained by using the strict calculation results of the three-particle model. Furthermore, we can explore special cases. If we think that it is almost impossible for two particles to occupy the same potential well, when choosing the lowest-energy band, we can abandon the multioccupied state and keep only the single-occupied state. In this way, the effective Hamiltonian of the single-occupied state can be obtained, which can greatly reduce the subsequent calculation, and obtain the parameters of the effective Hamiltonian of the single-occupied state more accurately than using the second-order perturbation theory.

ACKNOWLEDGMENTS

This work was supported by the National Natural Science Foundation of China (Grants No. 11625417, No. 11604107, No. 91636219, and No. 11727809) and the National Key Research and Development Program of China, Grants No. 2022YFC3003802.

-
- [1] M. Atala, M. Aidelsburger, J. T. Barreiro, D. Abanin, T. Kitagawa, E. Demler, and Immanuel Bloch, Direct measurement of the Zak phase in topological Bloch bands, *Nat. Phys.* **9**, 795 (2013).
 - [2] L. Tarruell, D. Greif, T. Uehlinger, G. Jotzu, and T. Esslinger, Creating, moving and merging Dirac points with a Fermi gas in a tunable honeycomb lattice, *Nature (London)* **483**, 302 (2012).
 - [3] X.-Q. Wang, G.-Q. Luo, J.-Y. Liu, G.-H. Huang, Z.-X. Li, C. Wu, A. Hemmerich, and Z.-F. Xu, Evidence for quantum stripe ordering in a triangular optical lattice, *Phys. Rev. Lett.* **131**, 226001 (2023).
 - [4] J. Yang, L. Liu, J. Mongkolkiattichai, and P. Schauss, Site-Resolved imaging of ultracold fermions in a triangular-lattice quantum gas microscope, *PRX Quantum* **2**, 020344 (2021).
 - [5] G. B. Jo, J. Guzman, C. K. Thomas, P. Hosur, A. Vishwanath, and D. M. Stamper-Kurn, Ultracold atoms in a tunable optical kagome lattice, *Phys. Rev. Lett.* **108**, 045305 (2012).
 - [6] P. J. Lee, M. Anderlini, B. L. Brown, J. Sebby-Strabley, W. D. Phillips, and J. V. Porto, Sublattice addressing and spin-dependent motion of atoms in a double-well lattice, *Phys. Rev. Lett.* **99**, 020402 (2007).
 - [7] J. Sebby-Strabley, M. Anderlini, P. S. Jessen, and J. V. Porto, Lattice of double wells for manipulating pairs of cold atoms, *Phys. Rev. A* **73**, 033605 (2006).
 - [8] T. Uehlinger, G. Jotzu, M. Messer, D. Greif, W. Hofstetter, U. Bissbort, and T. Esslinger, Artificial graphene with tunable interactions, *Phys. Rev. Lett.* **111**, 185307 (2013).
 - [9] K. L. Lee, B. Grémaud, R. Han, B.-G. Englert, and C. Miniatura, Ultracold fermions in a graphene-type optical lattice, *Phys. Rev. A* **80**, 043411 (2009).
 - [10] C. Chin, R. Grimm, P. Julienne, and E. Tiesinga, Feshbach resonances in ultracold gases, *Rev. Mod. Phys.* **82**, 1225 (2010).
 - [11] E. Timmermans, P. Tommasini, M. Hussein, and A. Kerman, Feshbach resonances in atomic Bose–Einstein condensates, *Phys. Rep.* **315**, 199 (1999).
 - [12] F. Schäfer, T. Fukuhara, S. Sugawa, Y. Takasu, and Y. Takahashi, Tools for quantum simulation with ultracold atoms in optical lattices, *Nat. Rev. Phys.* **2**, 411 (2020).
 - [13] C. Gross, and I. Bloch, Quantum simulations with ultracold atoms in optical lattices, *Science* **357**, 995 (2017).
 - [14] P. Scholl, M. Schuler, H. J. Williams, A. A. Eberharter, D. Barredo, K. N. Schymik, V. Lienhard, L.-P. Henry, T. C. Lang, T. Lahaye, A. M. Läuchli, and A. Browaeys, Quantum simulation of 2D antiferromagnets with hundreds of Rydberg atoms, *Nature (London)* **595**, 233 (2021).
 - [15] M. Greiner, O. Mandel, T. Esslinger, T. W. Hänsch, and I. Bloch, Quantum phase transition from a superfluid to a Mott insulator in a gas of ultracold atoms, *Nature (London)* **415**, 39 (2002).
 - [16] B. Song, S. Dutta, S. Bhave, J. C. Yu, E. Carter, N. Cooper, and U. Schneider, Realizing discontinuous quantum phase transitions in a strongly correlated driven optical lattice, *Nat. Phys.* **18**, 259 (2022).
 - [17] D. van Oosten, P. van der Straten, and H. T. C. Stoof, Quantum phases in an optical lattice, *Phys. Rev. A* **63**, 053601 (2001).
 - [18] C. Monroe, Quantum information processing with atoms and photons, *Nature (London)* **416**, 238 (2002).
 - [19] I. Ryabtsev, I. Beterov, D. Tretyakov, V. Entin, and E. Yakshina, Spectroscopy of cold rubidium Rydberg atoms for applications in quantum information, *Phys. Usp.* **59**, 196 (2016).

- [20] V. Kasper, D. González-Cuadra, A. Hegde, A. Xia, A. Dauphin, F. Huber, E. Tiemann, M. Lewenstein, F. Jendrzejewski, and P. Hauke, Universal quantum computation and quantum error correction with ultracold atomic mixtures, *Quantum Sci. Technol.* **7**, 015008 (2022).
- [21] T. M. Graham, Y. Song, J. Scott, C. Poole, L. Phuttitarn, K. Jooya *et al.*, Multi-qubit entanglement and algorithms on a neutral-atom quantum computer, *Nature (London)* **604**, 457 (2022).
- [22] M. P. A. Fisher, P. B. Weichman, G. Grinstein, and D. S. Fisher, Boson localization and the superfluid-insulator transition, *Phys. Rev. B* **40**, 546 (1989).
- [23] D. Jaksch, C. Bruder, J. I. Cirac, C. W. Gardiner, and P. Zoller, Cold bosonic atoms in optical lattices, *Phys. Rev. Lett.* **81**, 3108 (1998).
- [24] N. Marzari and D. Vanderbilt, Maximally localized generalized Wannier functions for composite energy bands, *Phys. Rev. B* **56**, 12847 (1997).
- [25] B. Vaucher, S. R. Clark, U. Dörner, and D. Jaksch, Fast initialization of a high-fidelity quantum register using optical superlattices, *New J. Phys.* **9**, 221 (2007).
- [26] M. Modugno and G. Pettini, Maximally localized Wannier functions for ultracold atoms in one-dimensional double-well periodic potentials, *New J. Phys.* **14**, 055004 (2012).
- [27] J. Ibañez-Azpiroz, A. Eiguren, A. Bergara, G. Pettini, and M. Modugno, Self-consistent tight-binding description of Dirac points moving and merging in two-dimensional optical lattices, *Phys. Rev. A* **88**, 033631 (2013).
- [28] R. Walters, G. Cotugno, T. H. Johnson, S. R. Clark, and D. Jaksch, *Ab initio* derivation of Hubbard models for cold atoms in optical lattices, *Phys. Rev. A* **87**, 043613 (2013).
- [29] J. Ibañez-Azpiroz, A. Eiguren, A. Bergara, G. Pettini, and M. Modugno, Tight-binding models for ultracold atoms in honeycomb optical lattices, *Phys. Rev. A* **87**, 011602(R) (2013).
- [30] C. Brouder, G. Panati, M. Calandra, C. Mourougane, and N. Marzari, Exponential localization of wannier functions in insulators, *Phys. Rev. Lett.* **98**, 046402 (2007).
- [31] S. Paul and E. Tiesinga, Wannier functions using a discrete variable representation for optical lattices, *Phys. Rev. A* **94**, 033606 (2016).
- [32] S. Kivelson, Wannier functions in one-dimensional disordered systems: Application to fractionally charged solitons, *Phys. Rev. B* **26**, 4269 (1982).
- [33] G. K. Campbell, J. Mun, M. Boyd, P. Medley, A. E. Leanhardt, L. G. Marcassa, D. E. Pritchard, and W. Ketterle, Imaging the mott insulator shells by using atomic clock shifts, *Science* **313**, 649 (2006).
- [34] B. J. Bloom, T. L. Nicholson, J. R. Williams, S. L. Campbell, M. Bishof, X. Zhang, W. Zhang, S. L. Bromley, and J. Ye, An optical lattice clock with accuracy and stability at the 10^{-18} level, *Nature (London)* **506**, 71 (2014).
- [35] S. Will, T. Best, U. Schneider, L. Hackermüller, D. Lühmann, and I. Bloch, Time-resolved observation of coherent multi-body interactions in quantum phase revivals, *Nature (London)* **465**, 197 (2010).
- [36] P. R. Johnson, D. Blume, X. Y. Yin, W. F. Flynn, and E. Tiesinga, Effective renormalized multi-body interactions of harmonically confined ultracold neutral bosons, *New J. Phys.* **14**, 053037 (2012).
- [37] O. Dutta, M. Gajda, P. Hauke, M. Lewenstein, D. S. Lühmann, B. A. Malomed, and J. Zakrzewski, Non-standard Hubbard models in optical lattices: A review, *Rep. Prog. Phys.* **79**, 116401 (2016).
- [38] M. Hughes, A. U. J. Lode, D. Jaksch, and P. Massignan, Accuracy of quantum simulators with ultracold dipolar molecules: A quantitative comparison between continuum and lattice descriptions, *Phys. Rev. A* **107**, 033323 (2023).
- [39] W. Beugeling, J. C. Everts, and C. Morais Smith, Topological phase transitions driven by next-nearest-neighbor hopping in two-dimensional lattices, *Phys. Rev. B* **86**, 195129 (2012).
- [40] D. Lühmann, O. Jürgensen, and K. Sengstock, Multi-orbital and density-induced tunneling of bosons in optical lattices, *New J. Phys.* **14**, 033021 (2012).
- [41] O. Jürgensen, F. Meinert, M. J. Mark, H. Nägerl, and D. Lühmann, Observation of density-induced tunneling, *Phys. Rev. Lett.* **113**, 193003 (2014).
- [42] X. F. Zhou, Y. S. Zhang, and G. C. Guo, Pair tunneling of bosonic atoms in an optical lattice, *Phys. Rev. A* **80**, 013605 (2009).
- [43] J. Q. Liang, J. L. Liu, W. D. Li, and Z. J. Li, Atom-pair tunneling and quantum phase transition in the strong-interaction regime, *Phys. Rev. A* **79**, 033617 (2009).
- [44] Q. Zhu, Q. Zhang, and B. Wu, Extended two-site Bose-Hubbard model with pair tunneling: Spontaneous symmetry breaking, effective ground state and fragmentation, *J. Phys. B* **48**, 045301 (2015).
- [45] M. J. Mark, E. Haller, K. Lauber, J. G. Danzl, A. J. Daley, and H. C. Nägerl, Precision measurements on a tunable mott insulator of ultracold atoms, *Phys. Rev. Lett.* **107**, 175301 (2011).
- [46] M. Łacki, D. Delande and J. Zakrzewski, Dynamics of cold bosons in optical lattices: Effects of higher Bloch bands, *New J. Phys.* **15**, 045021 (2013).
- [47] J. Major, J. M. Łacki, and J. Zakrzewski, Reexamination of the variational Bose-Hubbard model, *Phys. Rev. A* **89**, 043626 (2014).
- [48] P. R. Johnson, E. Tiesinga, J. V. Porto and C. J. Williams, Effective three-body interactions of neutral bosons in optical lattices, *New J. Phys.* **11**, 093022 (2009).
- [49] M. Singh, A. Dhar, T. Mishra, R. V. Pai, and B. P. Das, Three-body on-site interactions in ultracold bosonic atoms in optical lattices and superlattices, *Phys. Rev. A* **85**, 051604(R) (2012).
- [50] S. Mondal, A. Kshetrimayum, and T. Mishra, Two-body repulsive bound pairs in a multibody interacting Bose-Hubbard model, *Phys. Rev. A* **102**, 023312 (2020).
- [51] S. Zhu and B. Wu, Interaction effects on Wannier functions for bosons in an optical lattice, *Phys. Rev. A* **92**, 063637 (2015).
- [52] M. Kremer, R. Sachdeva, A. Benseny, and T. Busch, Interaction-induced effects on Bose-Hubbard parameters, *Phys. Rev. A* **96**, 063611 (2017).
- [53] W. Xu, M. Olshanii, and M. Rigol, Multiband effects and the Bose-Hubbard model in one-dimensional lattices, *Phys. Rev. A* **94**, 031601(R) (2016).
- [54] A. Pricoupenko and D. S. Petrov, Higher-order effective interactions for bosons near a two-body zero crossing, *Phys. Rev. A* **103**, 033326 (2021).
- [55] P.-O. Löwdin, On the nonorthogonality problem, *Adv. Quantum Chem.* **5**, 185 (1970).
- [56] E. Schmidt, Zur Theorie der linearen und nichtlinearen Integralgleichungen, *Math. Ann.* **64**, 161 (1907).

- [57] T. Kock, M. Ölschläger, A. Ewerbeck, W. M. Huang, L. Mathey, and A. Hemmerich, Observing chiral superfluid order by matter-wave interference, *Phys. Rev. Lett.* **114**, 115301 (2015).
- [58] Z. Xu, L. You, A. Hemmerich, and W. Vincent Liu, π -Flux dirac bosons and topological edge excitations in a bosonic chiral p -Wave superfluid, *Phys. Rev. Lett.* **117**, 085301 (2016).
- [59] Y. Ke, X. Qin, Y. S. Kivshar, and C. Lee, Multiparticle wannier states and thouless pumping of interacting bosons, *Phys. Rev. A* **95**, 063630 (2017).
- [60] W. C. Lu, C. Z. Wang, T. L. Chan, K. Ruedenberg, and K. M. Ho, Representation of electronic structures in crystals in terms of highly localized quasiatomic minimal basis orbitals, *Phys. Rev. B* **70**, 041101(R) (2004).